Knotting a tetrahedral cage mechanically locks guests inside

Yuchong Yang[1], Tanya K. Ronson[1], Paula C.P. Teeuwen[1], Simone Zucchelli[2], Andrew W. Heard[1], Paola Posocco[2], David J. Wales[1], Jonathan R. Nitschke*[, 1]

[1]Yusuf Hamied Department of Chemistry, University of Cambridge, Lensfield Road, Cambridge, CB2 1EW, UK.

[2]Department of Engineering and Architecture (DEA), University of Trieste, 34127 Trieste, Italy

*e-mail: jrn34@cam.ac.uk

Abstract

Interwoven molecular structures underpin the functions of many biomolecules,[1–3] yet synthesizing artificial topologically-complex structures in high yield remains challenging.[4,5] Here we describe a streamlined, high yield one-pot synthesis of knotted cage frameworks through the use of a subcomponent designed to bridge over the faces of a predesigned cage framework. A $Zn^{II}_4L_3$ open-faced cage framework was employed as the basis for a topologically chiral 'perplexane',[6] and a $Zn^{II}_4L_4$ tetrahedron was built into a topologically chiral 'trefoil tetrahedron'. Both interwoven architectures can be prepared through one-pot subcomponent self-assembly from a trialdehyde, the bridging triamine, and a zinc(II) salt. The 'trefoil tetrahedron' was observed to mechanically lock guests inside the cavity, resulting in a guest exchange half-life 17000 times longer than that of the original tetrahedral cage. Both cage frameworks were reduced and demetallated to yield metal-free interwoven structures, with the 'perplexane' producing an achiral product, and the 'trefoil tetrahedron' maintaining its topological chirality. Our strategy may enable the many existing cage frameworks produced using subcomponent self-assembly to be knotted, enhancing their robustness and locking guests inside.

Introduction

Weaving is one of the rare technologies that has enabled human progress since the dawn of civilization, from baskets and textiles,[7] to the interlaced structures of the latest synthetic molecular machines.[8] Complex topologies likewise underpin the functions of natural biomolecular structures, including proteins,[1] DNA,[2] and RNA.[3] Inspired by these natural systems, the Sauvage group first used metal templation to obtain macroscopic quantities of a trefoil knot.[9] Subsequently, a range of artificial interwoven structures with more complex topologies, such as catenanes,[10–13] molecular knots,[5] and Borromean rings,[14–16] have been developed through various strategies, including selective linking of the ends of interwoven grids,[17] hydrophobic effects,[18] and metal ion templation.[4,19–21] These topologically-complex assemblies have potential in applications such as ion transport,[22] catalysis,[23] and tailoring polymer properties.[24] While key design principles for such interwoven structures are now established, the development of higher-order, topologically complex architectures with bifurcated strands remains a challenge.[4] This difficulty arises primarily from the requirement for the preorganization of a stable framework, which must then be linked together in the precise way needed to give the desired topology, while avoiding linkages that produce different product structures, or mixtures.

Metal-coordination-driven self-assembly has emerged as a robust approach for synthesizing polyhedral metal-organic cages, encompassing structures such as Platonic and Archimedean solids,[25–29] along with prisms and antiprisms.[30,31] These polyhedral cages, with precise geometric configurations and enclosed internal cavities, are useful in applications including natural product encapsulation,[30] selective molecular separation and delivery,[32] sensing,[33] catalysis,[34] and the stabilization of reactive species.[35]

We hypothesized that an exterior crosslinking strategy, utilizing a well-defined metal-organic cage as the structural core, could promote the formation of interwoven structures with complex topologies, as shown in Figure 1. This approach aims to streamline the synthesis while simultaneously enhancing the complexity of the interwoven structure and overall yield of the process. Such a crosslinking strategy could also increase robustness through a greater density of connections between subunits, and hinder guest release via a more rigid and tangled framework for the escaping guest to navigate.

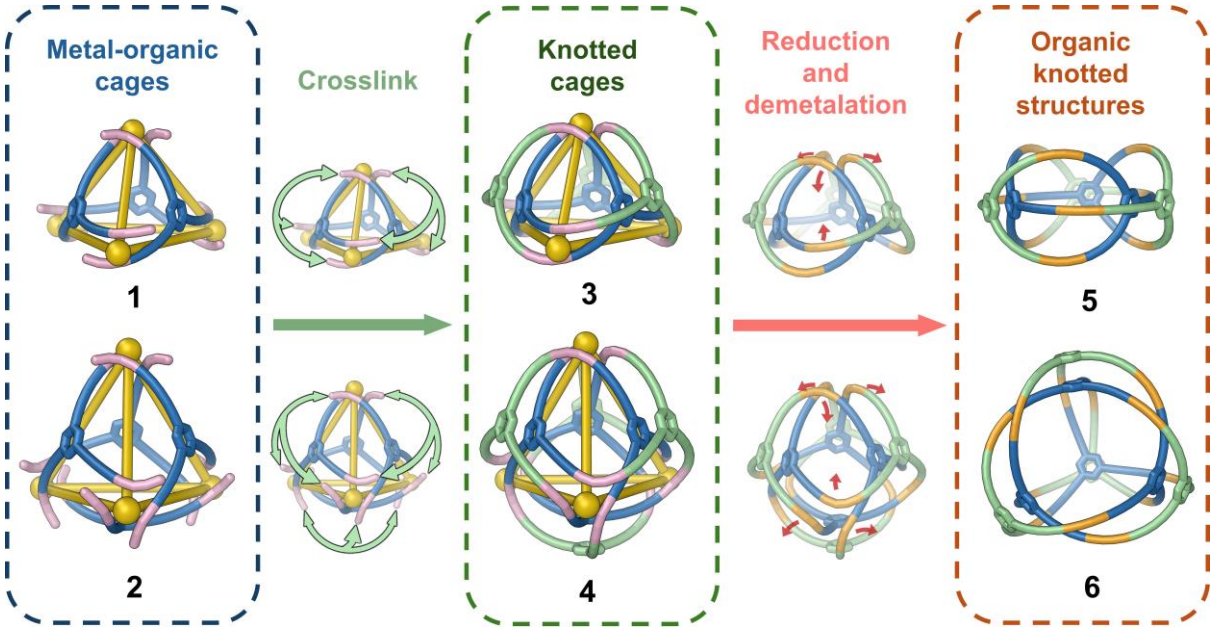

Figure 1. Exterior cross-linking strategy for the construction of knotted cages and organic covalent-interwoven structures. Cage frameworks **1** and **2** serve as scaffolds for crosslinking into knotted cages **3** and **4** through the addition of tritopic linkers. The dynamic-covalent imine bonds of these topologically complex structures may then be reduced into secondary amines, and the metal ions removed, in order to create metal-free organic perplexane **5** and knotted tetrahedron **6**.

Here we report a high yielding, one-pot preparation of interwoven three-dimensional structures **3** and **4** based on open-faced tetrahedron **1** and enclosed tetrahedron **2**, respectively. Both **2** and **4** were observed to bind anionic guests, but guest exchange for interwoven **4** was observed to take place 17000 times slower than in the case of its non-interwoven congener **2**. The added layer of crosslinked molecular strands rigidifies the cage and presents a mechanical barrier to guest exit, thereby locking the guest molecules within the cavity. This stronger guest retention could be useful in the context of delivery, where slow and controlled rates of release are necessary.

Both open-faced **3** and fully-enclosed **4** were reduced and demetallated to yield fully organic, covalently-linked interwoven structures **5** and **6**, respectively. Both **4** and **6** are chiral, with the topological chirality[36] of **6** being determined by the handedness of the chiral tetrahedral (*T* point group) framework of its precursor **4**. Although the framework of **3** has a handedness determined by the stereochemistry of its constituent metal centres, metal-free **5** is topologically achiral, as noted by Tilley et al.,[6] who referred to this topology as a 'perplexane'. As shown in in the upper right of Figure 1, the branches of **5** can adopt an achiral C_{3h}-symmetric configuration with a central mirror plane. Our method thus allows access to topologically chiral and achiral products from the same set of precursors.

Results and discussion

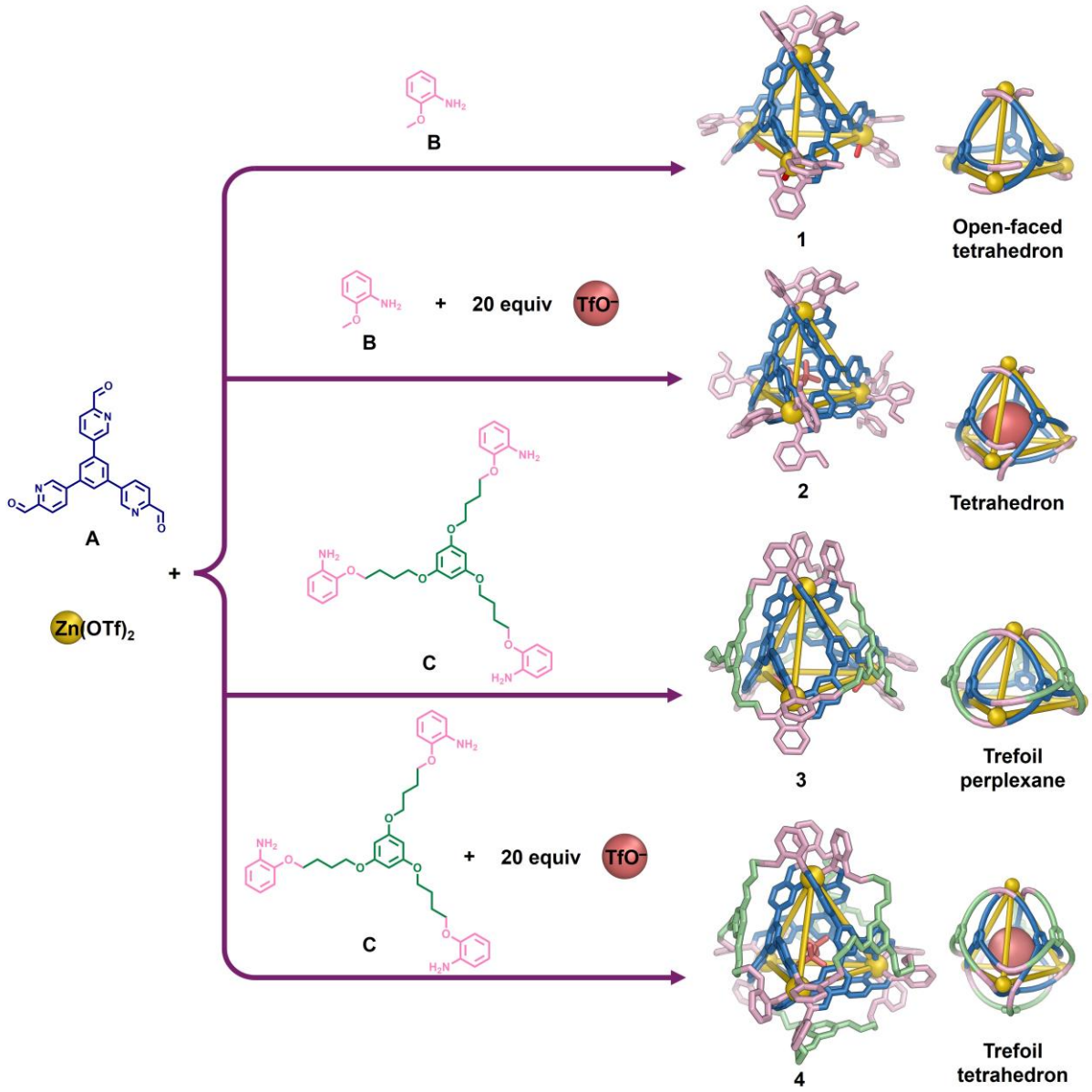

Figure 2. Subcomponent self-assembly of tetrahedral structures 1, 2, 3 and 4. *O*-anisidine **A** reacted with trialdehyde **B** and zinc(II) triflate to generate open-faced **1**, or enclosed **2** in the

presence of excess triflate. Tritopic triamine **C,** bridged over the tetrahedron faces formed from **A** residues, produces interwoven open-faced **3** and fully-enclosed **4**, again in the presence of excess triflate.

As shown in Figure 2, trialdehyde **A** (3 equiv) and zinc(II) trifluoromethanesulfonate (triflate or TfO^-, 4 equiv) reacted with *o*-anisidine **B** (9 equiv) or triamine **C** (3 equiv) in acetonitrile to produce open-faced assemblies **1** and **3**, respectively. The solution-phase structure of **1** was confirmed through nuclear magnetic resonance (NMR) spectroscopy and electrospray ionization mass spectrometry (ESI-MS), which both gave results consistent with an open-faced $Zn^{II}_4L_3$ tetrahedron, as shown in Figures S3-S11. Analysis of the ^{1}H NMR and heteronuclear single quantum coherence (HSQC) spectra (Figures S3 and S8) showed three distinct sets of resonances, consistent with a C_3-symmetric framework. ^{1}H NMR Diffusion-ordered spectroscopy (DOSY) indicated the presence of a single species with a hydrodynamic radius of 12.8 Å (Figure S9). This radius is consistent with the GFN-FF[37] minimized structure of **1**, based on the crystal structure of **3** (Figure 2). All four Zn^{II} centres have the same handedness, with $Zn^{II}\cdots Zn^{II}$ distances ranging from 11.4 to 12.2 Å. The observed stoichiometry incorporates one tris(pyridylimine)-chelated Zn^{II} vertex and three bis(pyridylimine) Zn^{II} vertices. Thus, only three of the four faces are covered by ligands, forming an open-faced tetrahedron. A similar open-faced geometry was reported by Shionoya et al.,[38] attributed to the coordinative flexibility of Zn^{II}.

Tritopic subcomponent **C** joins three anisidine residues covalently in a configuration that we hypothesized would bridge over the faces of a tetrahedral framework, thus resulting in a topologically complex interwoven structure. The formation of open-faced interwoven tetrahedron **3** (Figure 2) confirmed this hypothesis. The structure of **3** was confirmed by NMR spectroscopy and ESI-MS, as shown in Figures S22-S31. DOSY ^{1}H NMR (Figure S29) gave a solvodynamic radius of 12.8 Å for **3**. This radius was consistent with the size of **3** obtained in the solid-state, as determined by single-crystal X-ray diffraction (XRD) at the Diamond Light Source synchrotron.[39]

Complex **3** exhibits C_3 point group symmetry, as reflected in its NMR spectra (Figure S27). From the top view of **3** (Figure 3b), a trefoil knot can be traced as the shortest path through the cage framework, as illustrated by the red line in Figure 3b, thus forming a trefoil perplexane [6] structure or a branched trefoil knot framework. Compound **3** therefore possesses a continuous graph, with a single bifurcating molecular strand woven around the four templating Zn^{II} centres.

The $Zn^{II}\cdots Zn^{II}$ distances between adjacent metal centres range from 10.6 Å to 11.4 Å, as shown in Figure 3a. As with **1**, **3** incorporates one tris(pyridylimine)-chelated Zn^{II} vertex and three bis(pyridylimine) chelated Zn^{II} vertices, resulting in one open face (Figure 2), reflecting the underlying cage framework shared with **1**. All four Zn^{II} vertices within **3** have the same handedness, with both Δ_4 and Λ_4 enantiomers related by inversion in the crystal.

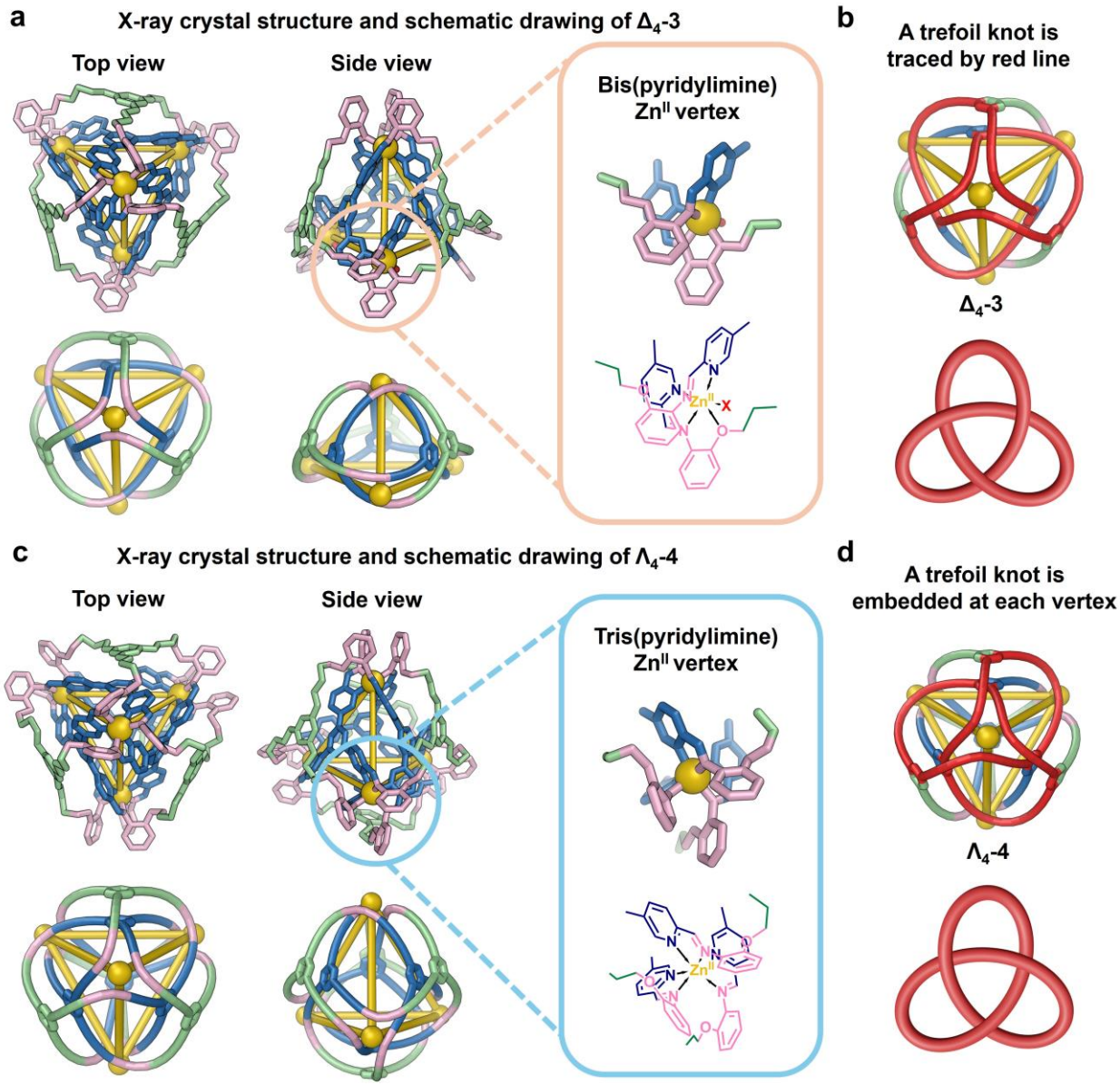

Figure 3. X-ray crystal structures of 3 and 4. Top and side views of both structures are shown above schematic views illustrating their topology. Disorder, hydrogen atoms, counterions and solvent molecules of crystallization are omitted for clarity; **a)** the structure of **3** contains three bis(pyridylimine) vertices with an additional counterion (shown as a red 'X' in the expansion) bound to zinc, and one tris(pyridylimine) apical vertex, lending it non-crystallographic C_3 point group symmetry; **b)** the shortest closed path along the ligand (shown in red) describes a trefoil knot; **c)** structure **4** has idealised chiral tetrahedral (*T*) point group symmetry, with all tris(pyridylimine)zinc vertices coordinatively saturated; **d)** trefoil knot motifs are similarly embedded at each vertex of **4**.

Metal-organic cage receptors can reconfigure to bind guests[40,41]. We therefore explored the addition of excess TfO^- (20 equiv) as a template during cage synthesis. In place of **1** or **3**, this triflate was found to drive the formation of coordinatively-saturated structure **2** or **4**, as shown in Figure 2, by binding within the cage cavity.

The tetrahedral structure of **2** was confirmed by NMR spectroscopy and ESI-MS, as shown in Figures S12-S21. DOSY ^{1}H NMR analysis of **2** revealed a hydrodynamic radius of 12.5 Å (Figure S19), consistent with a tetrahedral framework. The ^{19}F NMR spectrum of **2** exhibited signals corresponding to both free and encapsulated TfO^- (Figure S14), consistent with TfO^- templating the formation of the framework of **2** by binding inside its cavity. We infer that all faces of **2** are covered by ligands, similar to a previously reported tetrahedral cage[42] prepared from **A**, as shown in Figure 2. We infer the enclosed cavity of **2** serves as a more favourable host for triflate than the open bowl-shaped cavity of **1**. All data are consistent with *T* point symmetry for **2**, with all metal centres of a single handedness within each cage (Figures S12 and S17).

Using a similar strategy, knotted tetrahedron **4** was constructed through the assembly of zinc(II) with tritopic subcomponents **A** and **C** in the presence of excess triflate. This approach yielded a topologically intricate structure where the tetrahedral core of **2** was crosslinked by **C** residues. NMR spectroscopy and ESI-MS provided results consistent with the presence of an interwoven tetrahedral framework, as shown in Figures S32-S41. Only one environment per ligand proton of **4** was observed in the ^{1}H NMR spectrum, as with **2**. DOSY NMR gave a solvodynamic radius of 12.8 Å (Figure S39), consistent with the crystal structure of **4**.

Single-crystal X-ray diffraction at Diamond Light Source[39] confirmed the structure of **4**, as shown in Fig 3c, containing four tris-pyridyl(imine) chelated Zn^{II} centres bridged by a continuous double-layered woven ligand. The inner core of the structure is analogous to previously reported M_4L_4 cages prepared from **A**, with the outer ligand linking each of the three adjacent faces, resulting in the formation of a single knotted ligand wrapping around the four zinc vertices. Looking down the C_3 axis of each vertex, a trefoil knot can be traced as the shortest circular path along the ligand, as illustrated by the red line in Figure 3d. The $Zn^{II}\cdots Zn^{II}$ distances between adjacent Zn^{II} centres were observed to range from 11.4 Å to 11.6 Å. All vertices again have the same Δ or Λ handedness, with *T* point group symmetry. Although **4** was observed to crystallize in the chiral space group $P2_12_12_1$ as a racemic twin, we infer that in the bulk **4** exists as a racemic mixture of two topologically chiral enantiomers (Figure 3d). The crystal structure also reveals that a TfO^- anion is encapsulated within the cavity of **4** (Figure S76), consistent with the data obtained from the ^{19}F NMR spectra (Figure S34), which is also consistent with TfO^- adopting the role of template during the synthesis of **4**.

Guest binding affinity is critical in determining the functional utility of host molecules[43–45]. However, the stable encapsulation of guests with weak binding affinities remains a challenge in host-guest chemistry. We hypothesized that the interwoven framework of **4** might rigidify the cage and present a mechanical barrier to guest exit, thus offering an effective strategy to enhance the stabilization of bound guests.

The guest exchange behaviour of knotted cage **4** was investigated, with its congener **2** serving as a control. Previous studies[42] have shown that ReO_4^- binds with ca. 100-fold greater affinity than TfO^- within tetrahedral cages sharing the same framework as **2** and **4**. To probe guest exchange, excess ReO_4^- was added to solutions of $TfO^-\subset$**2** and $TfO^-\subset$**4**, and guest exchange was monitored via ^{1}H NMR spectroscopy. New ^{1}H NMR peaks corresponding to the perrhenate adducts were

observed, and the ^{19}F NMR peaks corresponding to encapsulated triflate disappeared, during guest exchange (Figures S42 - S48).

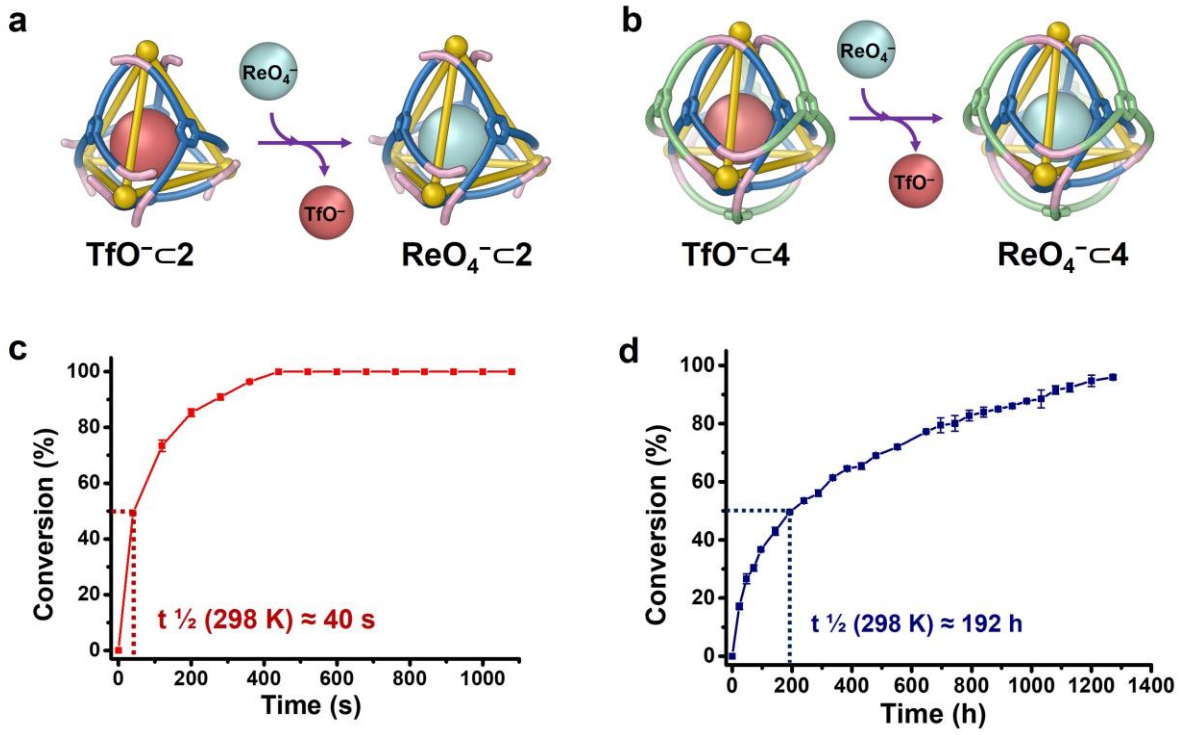

Figure 4. Comparison of anionic guest exchange between 2 and 4. Schematic illustrations of the displacement of TfO^- by ReO_4^- within **a)** cage **2**; and **b)** cage **4**. **c)** and **d)** show the traces of these processes within **2** and **4**, respectively, as monitored by ^1H NMR.

Different guest displacement rates were observed for $TfO^-\subset$**2** and $TfO^-\subset$**4** upon the addition of ReO_4^- in the presence of a total of 28 equiv of TfO^-. As shown in Figure 4, the addition of ReO_4^- to a solution of $TfO^-\subset$**2** resulted in a rapid increase in the ^1H NMR signals corresponding to $ReO_4^-\subset$**2**, while the signals for $TfO^-\subset$**2** diminished concurrently. In contrast, the ^1H NMR signals for $ReO_4^-\subset$**4** increased at a significantly slower rate under identical conditions. The half-life ($t_{1/2}$) for conversion of $TfO^-\subset$**2** into $ReO_4^-\subset$**2** was measured to be 40 s, whereas the $TfO^-\subset$**4** to $ReO_4^-\subset$**4** conversion required 192 hours to reach the same conversion level under identical conditions. The knotting of the cage framework of **4** thus reduced the rate of anionic guest exchange by a factor of 17000.

To quantify how the woven structure of **4** mechanically restricts the dynamic motion of its tetrahedral core during guest exchange, the enthalpy ($\Delta H^{\ddagger}$) and entropy ($\Delta S^{\ddagger}$) of activation for the substitution of perrhenate for triflate within **2** and **4** were analysed using the Eyring equation (Figures S53-S56). The enthalpy of activation for **2** (49.5 ± 2.4 kJ·mol^{-1}) was less than for **4** (65.1 ± 2.4 kJ·mol^{-1}), consistent with a more rigid host framework for **4**, with a higher barrier to deformation. The entropy of activation is likewise less favourable for **4** (-141.0 ± 9.9 J·mol^{-1}·K^{-1}) than for **2** (-113.1 ± 11.5 J·mol^{-1}·K^{-1}), consistent with a more rigid and tangled framework for the

escaping guest to navigate within **4**. Arrhenius analysis (Figure S57) further confirmed a higher activation energy and less favourable pre-exponential factor in the case of **4**.

Molecular dynamics (MD) simulations were conducted using a CHARMM general force field[46] to analyse the dynamics of **2** and **4** relevant to guest exchange. As shown in Figure S80, the apertures within the interior tetrahedral core of **4** exhibit a reduced proton-proton distance between adjacent faces compared to those in framework **2**, corresponding to a decrease of approximately 0.3 Å in largest aperture width. These observations indicated that the steric hindrance imparted by the woven ligand framework mechanically suppresses the dynamic motion of the tetrahedral core of **4**, inducing a contraction in average aperture size. This reduction in aperture[47] is likely to decrease the frequency of effective collisions between $ReO_4^-$and $TfO^-\subset$**2**, thereby more effectively trapping TfO^- within the cavity.

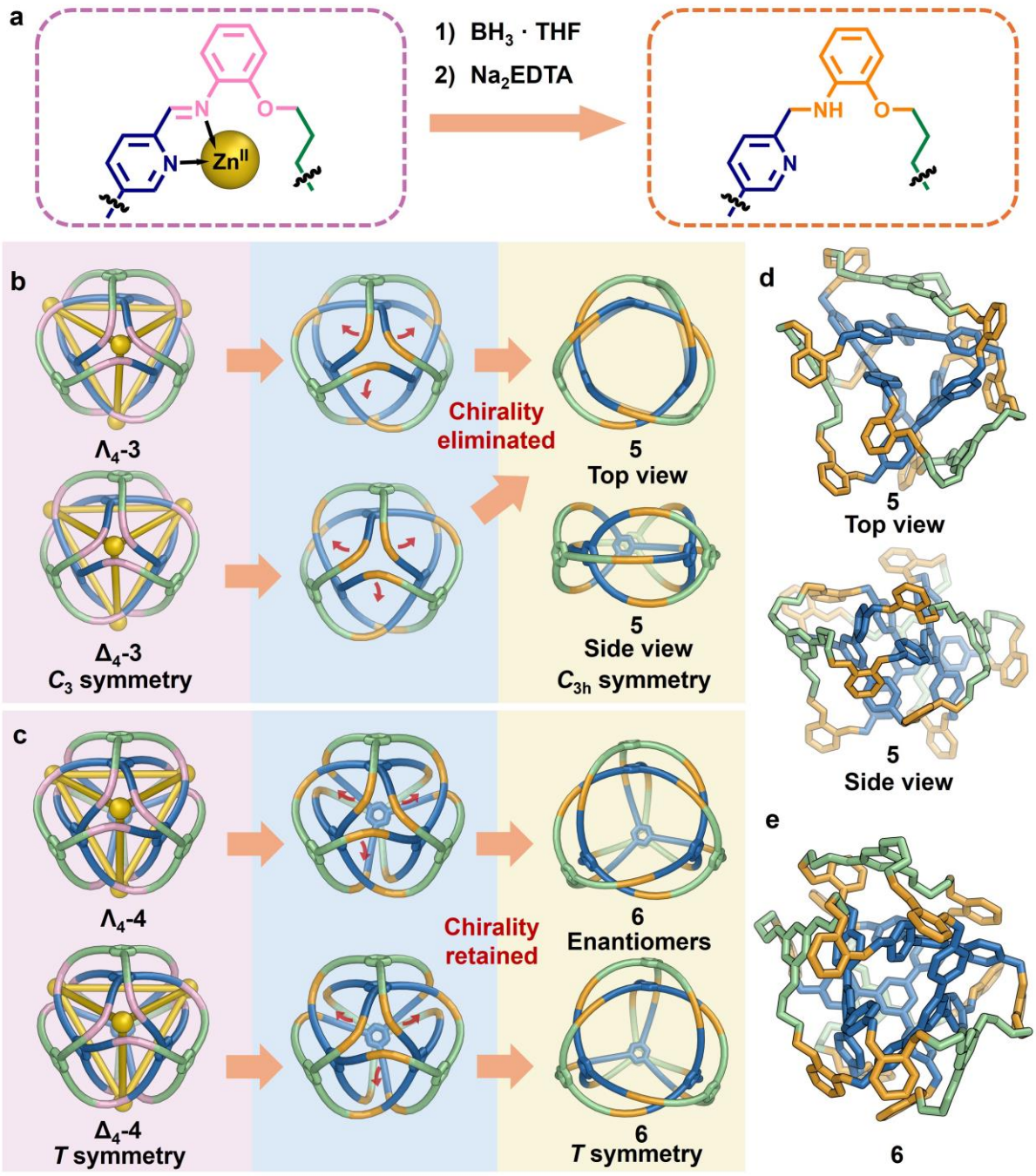

Figure 5. Preparation of 5 and 6. a) Reduction and demetallation of the imine bonds in **3** and **4**; Schematic illustrations of reduction and demetallation of **b) 3** and **c) 4**; **d)** GFN2-xTB[48]-optimized structure of **5**, calculated using GMIN; **e)** GFN2-xTB[48]-optimized structure of **6** (from Δ_4-**4**), determined with GMIN**.**

As shown in Figure 5, we explored the reduction and demetallation of **3** and **4** to obtain the fully organic covalent-interwoven structures **5** and **6**, which proceeded with yields of 87% and 55%, respectively. The stereochemistry of the Zn^{II} centres of **3** led to the formation of a racemic mixture of two enantiomers, as shown in Figure 5b. However, this chirality was eliminated during reduction and demetallation, yielding achiral organic trefoil perplexane, **5** (Figure 5b), with time-averaged C_{3h} symmetry. Treatment of **3** with BH_3·THF and Na_2EDTA in a mixed acetonitrile/methanol solution transformed the dynamic imine linkages into stable secondary amines, as confirmed by NMR spectra and Matrix-Assisted Laser Desorption/Ionization Time-of-Flight (MALDI-TOF) mass spectrometry (Figures S58-S65). DOSY ^{1}H NMR gave a solvodynamic radius of 8.4 Å (Figure S64), which was consistent with the minimized structure of **5**, which was obtained via basin-hopping[49] global optimization using the GMIN programme at the GFN-FF[37] level followed by geometry optimizations at the GFN2-xTB[48] level, as shown in Fig 5d.

The four zinc(II) vertices of trefoil tetrahedron **4** possess either all Δ or all Λ handedness, with **4** forming as a racemic mixture of its two enantiomers. In contrast to **3**, the chirality of **4** is topological in nature, being linked to the specific over/under pathways followed by its ligand strands as they weave together. In contrast to the chirality elimination observed in the transformation from **3** to **5**, this topological chirality of **4** is preserved even after reduction and demetallation (Figure 5c). This procedure thus yields the fully covalently linked organic trefoil tetrahedron **6** (Figure 5c). In contrast with elegant peptide-based structures reported by Fujita et al.,[50] the structure of **6**, along with that of its precursor **4**, possesses topology that is established along covalent-bond pathways, without considering any labile coordinative bonds. The structure of **6** was confirmed by NMR spectroscopy and MALDI-TOF mass spectrometry (Figures S66-S73). Only one environment per ligand proton of **6** was observed in the ^{1}H NMR spectrum, as with **4**, suggesting that the *T*-symmetric structure of **4** was retained in **6**, as shown in Figure S66. The ^{1}H DOSY spectrum of **6** indicated a solvodynamic radius of 11.2 Å (Figure S72). As shown in Figure 5e, the optimized geometry of **6** was obtained using GMIN at the GFN-FF[37] level, followed by further optimizations at the GFN2-xTB[48] level, producing a compact structure consistent in size with our DOSY results.

Conclusion

The construction of interwoven knotted cages **3** and **4**, using a simple, one-pot, high-yielding procedure underscores the effectiveness of subcomponent self-assembly in creating entangled, topologically-complex species. Our design strategy of bridging over the panels of metal-organic cage cores could be extended for construction of other novel interwoven frameworks. Based upon the observation that knotting causes cage **4** to release its guest 17000 times more slowly than non-knotted congener **2**, these cages may find use in controlled-release applications. The transformations of **3** and **4** into fully covalently linked structures **5** and **6** also reveal the utility of

our methods to prepare metal-free complex knotted structures, with the topological chirality of structures such as **5** potentially leading to new applications in chiral recognition. Future work will probe these applications, as well as the transfer of stereochemical information during the formation and reduction of these structures. The ability to control the geometric configuration and topological chirality of these structures will advance the design of novel woven materials and molecular devices.

Data availability

All data needed to evaluate the conclusions given in the paper are present in the paper and Supporting Information. Any additional data related to this paper may be requested from the authors. Crystallographic data for the structure reported in this paper has been deposited at the Cambridge Crystallographic Data Centre (deposition numbers 2415403 for **3** and 2415402 for **4**) and can be obtained free of charge via www.ccdc.cam.ac.uk/data_request/cif.

Acknowledgements:

This work was supported by the Defense Advanced Research Projects Agency (DARPA) MIMS program cooperative agreement HR00112420301. The views, opinions and/or findings expressed are those of the author and should not be interpreted as representing the official views or policies of the Department of Defense or the U.S. Government. This study was also supported by the European Research Council (695009) and the UK Engineering and Physical Sciences Research Council (EPSRC, EP/T031603/1, EP/S024220/1). We thank the Department of Chemistry NMR facility, University of Cambridge, for performing some NMR experiments, the EPSRC UK National Mass Spectrometry Facility at Swansea University for carrying out MALDI-TOF mass spectrometry and Diamond Light Source (UK) for synchrotron beamtime on I19 (CY29890). S.Z. and P.P. are also grateful to the Italian Ministry of University and Research for financial support under the National Recovery and Resilience Plan (NRRP) and to CINECA under the ISCRA initiative for high-performance computing resources and support.

Author Contributions:

J.R.N. and Y.Y. conceived the project and designed the experiments. Y.Y. performed the experiments and analysed the data. T.K.R. collected the X-ray data and refined the crystal structures. P.C.P.T. and D.J.W. performed the GFN-FF and GFN2-xTB calculations. P.C.P.T., S.Z. and P.P. performed the MD simulations. A.W.H. helped with MS measurements and discussed the chirality of structures. J.R.N. is the principal investigator. All authors discussed the results and commented on the manuscript.

References

1. Sułkowska, J. I.; Rawdon, E. J.; Millett, K. C.; Onuchic, J. N.; Stasiak, A. Conservation of complex knotting and slipknotting patterns in proteins. *Proc. Natl. Acad. Sci. USA* 2012, 109, E1715–E1723.
2. Wasserman, S. A., Cozzarelli, N. R. Biochemical topology: Applications to DNA recombination and replication. *Science* 1986, 232, 951–960.
3. Wikoff, W. R.; Liljas, L.; Duda, R. L.; Tsuruta, H.; Hendrix, R. W.; Johnson, J. E.

Topologically linked protein rings in the bacteriophage HK97 capsid. *Science* 2000, 289, 2129–2133.
4. Wu, L.; Tang, M.; Jiang, L.; Chen, Y.; Bian, L.; Liu, J.; Wang, S.; Liang, Y.; Liu, Z. Synthesis of contra-helical trefoil knots with mechanically tuneable spin-crossover properties. *Nat. Synth.* 2022, 2, 17–25.
5. Ashbridge, Z.; Fielden, S. D. P.; Leigh, D. A.; Pirvu, L.; Schaufelberger, F.; Zhang, L. Knotting matters: Orderly molecular entanglements. *Chem. Soc. Rev.* 2022, 51, 7779–7809.
6. Bergman, H. M.; Fan, A.; Jones, C. G.; Rothenberger, A. J.; Jha, K. K.; Handford, R. C.; Nelson, H. M.; Liu, Y.; Tilley, T. D. A new topological class of interlocked and interwoven nanocarbons via dynamic C-C bond formation. 2024, preprint at https://doi.org/10.26434/chemrxiv-2024-bvxjg-v2.
7. Postrel, V. The fabric of civilization: How textiles made the world. (Basic Books, 2020).
8. Zhang, L.; Marcos, V.; Leigh, D. A. Molecular machines with bio-inspired mechanisms. *Proc. Natl. Acad. Sci. USA* 2018, 115, 9397–9404.
9. Dietrich-Buchecker, C. O.; Sauvage, J. A synthetic molecular trefoil knot. *Angew. Chem. Int. Ed.* 1989, 28, 189–192.
10. Prakasam, T.; Lusi, M.; Elhabiri, M.; Platas-Iglesias, C.; Olsen, J.; Asfari, Z.; Cianférani-Sanglier, S.; Debaene, F.; Charbonnière, L. J.; Trabolsi, A. Simultaneous self-assembly of a [2]catenane, a trefoil knot, and a Solomon link from a simple pair of ligands. *Angew. Chem. Int. Ed.* 2013, 52, 9956–9960.
11. Wood, C. S.; Ronson, T. K.; Belenguer, A. M.; Holstein, J. J.; Nitschke, J. R. Two-stage directed self-assembly of a cyclic [3]catenane. *Nat. Chem.* 2015, 7, 354–358.
12. Li, H.; Zhang, H.; Lammer, A. D.; Wang, M.; Li, X.; Lynch, V. M.; Sessler, J. L. Quantitative self-assembly of a purely organic three-dimensional catenane in water. *Nat. Chem.* 2015, 7, 1003–1008.
13. Liu, Y.; O'Keeffe, M.; Treacy, M. J. M.; Yaghi, O. M. The geometry of periodic knots, polycatenanes and weaving from a chemical perspective: a library for reticular chemistry. *Chem. Soc. Rev.* 2018, 47, 4642–4664.
14. Chichak, K. S.; Cantrill, S. J.; Pease, A. R.; Chiu, S.-H.; Cave, G. W. V.; Atwood, J. L.; Stoddart, J. F. Molecular Borromean rings. *Science* 2004, 304, 1308–1312.
15. Zhu, R.; Lübben, J.; Dittrich, B.; Clever, G. H. Stepwise halide-triggered double and triple catenation of self-assembled coordination cages. *Angew. Chem. Int. Ed.* 2015, 54, 2796–2800.
16. Schalley, C. A. Borromean rings: A one-pot synthesis. *Angew. Chem. Int. Ed.* 2004, 43, 4399–4401.
17. Leigh, D. A.; Danon, J. J.; Fielden, S. D. P.; Lemonnier, J.-F.; Whitehead, G. F. S.; Woltering, S. L. A molecular endless (74) knot. *Nat. Chem.* 2021, 13, 117–122.
18. Cougnon, F. B. L.; Caprice, K.; Pupier, M.; Bauzá, A.; Frontera, A. A strategy to synthesize molecular knots and links using the hydrophobic effect. *J. Am. Chem. Soc.* 2018, 140, 12442–12450.
19. Carpenter, J. P.; McTernan, C. T.; Greenfield, J. L.; Lavendomme, R.; Ronson, T. K.; Nitschke, J. R. Controlling the shape and chirality of an eight-crossing molecular knot. *Chem* 2021, 7, 1534–1543.
20. Liu, Y.; Ma, Y.; Zhao, Y.; Sun, X.; Gándara, F.; Furukawa, H.; Liu, Z.; Zhu, H.; Zhu, C.;

Suenaga, K.; Oleynikov, P.; Alshammari, A. S.; Zhang, X.; Terasaki, O.; Yaghi, O. M. Weaving of organic threads into a crystalline covalent organic framework. *Science* 2016, 351, 365–369.
21. Leigh, D. A.; Schaufelberger, F.; Pirvu, L.; Stenlid, J. H.; August, D. P.; Segard, J. Tying different knots in a molecular strand. *Nature* 2020, 584, 562–568.
22. August, D. P.; Borsley, S.; Cockroft, S. L.; della Sala, F.; Leigh, D. A.; Webb, S. J. Transmembrane ion channels formed by a star of David [2]catenane and a molecular pentafoil knot. *J. Am. Chem. Soc.* 2020, 142, 18859–18865.
23. Prakasam, T.; Devaraj, A.; Saha, R.; Lusi, M.; Brandel, J.; Esteban-Gómez, D.; Platas-Iglesias, C.; Olson, M. A.; Mukherjee, P. S.; Trabolsi, A. Metal-organic self-assembled trefoil knots for C─Br bond activation. *ACS Catal.* 2019, 9, 1907–1914.
24. Zhang, M.; Nixon, R.; Schaufelberger, F.; Pirvu, L.; De Bo, G.; Leigh, D. A. Mechanical scission of a knotted polymer. *Nat. Chem.* 2024, 16, 1366–1372.
25. Olenyuk, B.; Levin, M. D.; Whiteford, J. A.; Shield, J. E.; Stang, P. J. Self-assembly of nanoscopic dodecahedra from 50 predesigned components. *J. Am. Chem. Soc.* 1999, 121, 10434–10435.
26. Wang, H.; Wang, K.; Xu, Y.; Wang, W.; Chen, S.; Hart, M.; Wojtas, L.; Zhou, L.-P.; Gan, L.; Yan, X.; Li, Y.; Lee, J.; Ke, X.-S.; Wang, X.-Q.; Zhang, C.-W.; Zhou, S.; Zhai, T.; Yang, H.-B.; Wang, M.; He, J.; Sun, Q.-F.; Xu, B.; Jiao, Y.; Stang, P. J.; Sessler, J. L.; Li, X. Hierarchical self-assembly of nanowires on the surface by metallo-supramolecular truncated cuboctahedra. *J. Am. Chem. Soc.* 2021, 143, 5826–5835.
27. Fujita, D.; Ueda, Y.; Sato, S.; Yokoyama, H.; Mizuno, N.; Kumasaka, T.; Fujita, M. Self-assembly of $M_{30}L_{60}$ icosidodecahedron. *Chem* 1, 91–101 (2016).
28. Koo, J.; Kim, I.; Kim, Y.; Cho, D.; Hwang, I.-C.; Mukhopadhyay, R. D.; Song, H.; Ko, Y. H.; Dhamija, A.; Lee, H.; Hwang, W.; Kim, S.; Baik, M.-H.; Kim, K. Gigantic porphyrinic cages. *Chem* 2020, 6, 3374–3384 (2020).
29. Wu, K.; Ronson, T. K.; Su, P.; Chen, Z.; Goh, L.; Heard, A. W.; Li, X.; Klautzsch, F.; Schalley, C. A.; Vinković, M.; Nitschke, J. R. Systematic construction of progressively larger capsules from a fivefold linking pyrrole-based subcomponent. *Nat. Synth.* 2023, 2, 789–797.
30. Rizzuto, F. J.; Carpenter, J. P.; Nitschke, J. R. Multisite binding of drugs and natural products in an entropically favorable, heteroleptic receptor. *J. Am. Chem. Soc.* 2019, 141, 9087–9095.
31. Sudan, S.; Li, R.-J.; Jansze, S. M.; Platzek, A.; Rudolf, R.; Clever, G. H.; Fadaei-Tirani, F.; Scopelliti, R.; Severin, K. Identification of a heteroleptic $Pd_6L_6L'_6$ coordination cage by screening of a virtual combinatorial library. *J. Am. Chem. Soc.* 2021, 143, 1773–1778.
32. Zhang, D.; Ronson, T. K.; Zou, Y.-Q.; Nitschke, J. R. Metal–organic cages for molecular separations. *Nat. Rev. Chem.* 2021, 5, 168–182.
33. Kreno, L. E.; Leong, K.; Farha, O. K.; Allendorf, M.; Van Duyne, R. P.; Hupp, J. T. Metal-organic framework materials as chemical sensors. *Chem. Rev.* 2012, 112, 1105–1125.
34. Saha, R.; Mondal, B.; Mukherjee, P. S. Molecular cavity for catalysis and formation of metal nanoparticles for use in catalysis. *Chem. Rev.* 2022, 122, 12244–12307.
35. Mal, P.; Breiner, B.; Rissanen, K.; Nitschke, J. R. White phosphorus is air-stable within a self-assembled tetrahedral capsule. *Science* 2009, 324, 1697–1699.
36. Forgan, R. S.; Sauvage, J.-P.; Stoddart, J. F. Chemical topology: Complex molecular knots,

links, and entanglements. *Chem. Rev.* 2011, 111, 5434–5464.
37. Spicher, S.; Grimme, S. Robust atomistic modeling of materials, organometallic, and biochemical systems. *Angew. Chem. Int. Ed.* 2020, 59, 15665−15673.
38. Endo, K.; Ube, H.; Shionoya, M. Multi-stimuli-responsive interconversion between bowl- and capsule-shaped self-assembled zinc(II) complexes. *J. Am. Chem. Soc.* 2020, 142, 407–416.
39. Allan, D. R.; Nowell, H.; Barnett, S. A.; Warren, M. R.; Wilcox, A.; Christensen, J.; Saunders, L. K.; Peach, A.; Hooper, M. T.; Zaja, L.; Patel, S.; Cahill, L.; Marshall, R.; Trimnell, S.; Foster, A. J.; Bates, T.; Lay, S.; Williams, M. A.; Hathaway, P. V; Winter, G.; Gerstel, M.; Wooley, R. W. A novel dual air-bearing fixed-χ diffractometer for small-molecule single-crystal x-ray diffraction on beamline I19 at Diamond Light Source. *Crystals* 2017, 7, 336.
40. Mirtschin, S.; Slabon-Turski, A.; Scopelliti, R.; Velders, A. H.; Severin, K. A coordination cage with an adaptable cavity size. *J. Am. Chem. Soc.* 2010, 132, 14004–14005.
41. Freye, S.; Michel, R.; Stalke, D.; Pawliczek, M.; Frauendorf, H.; Clever, G. H. Template control over dimerization and guest selectivity of interpenetrated coordination cages. *J. Am. Chem. Soc.* 2013, 135, 8476-8479.
42. Castilla, A. M.; Ronson, T. K.; Nitschke, J. R. Sequence-dependent guest release triggered by orthogonal chemical signals. *J. Am. Chem. Soc.* 2016, 138, 2342–2351.
43. Lehn, J.-M. Supramolecular chemistry: Receptors, catalysts, and carriers. *Science* 1985, 227, 849–856.
44. Zhu, H.; Chen, L.; Sun, B.; Wang, M.; Li, H.; Stoddart, J. F.; Huang, F. Applications of macrocycle-based solid-state host-guest chemistry. *Nat. Rev. Chem.* 2023, 7, 768–782.
45. Geng, W.-C.; Sessler, J. L.; Guo, D.-S. Supramolecular prodrugs based on host-guest interactions. *Chem. Soc. Rev.* 2020, 49, 2303–2315.
46. Vanommeslaeghe, K.; Hatcher, E.; Acharya, C.; Kundu, S.; Zhong, S.; Shim, J.; Darian, E.; Guvench, O.; Lopes, P.; Vorobyov, I.; Mackerell, A. D. CHARMM general force field: A force field for drug-like molecules compatible with the CHARMM all-atom additive biological force fields. *J. Comput. Chem.* 2010, 31, 671–690.
47. Pluth, M. D.; Raymond, K. N. Reversible guest exchange mechanisms in supramolecular host–guest assemblies. *Chem. Soc. Rev.* 2007, 36, 161–171.
48. Bannwarth, C.; Ehlert, S.; Grimme, S. GFN2-xTB—An accurate and broadly parametrized self-consistent tight-binding quantum chemical method with multipole electrostatics and density-dependent dispersion contributions. *J. Chem. Theory Comput.* 2019, 15, 1652–1671.
49. Wales, D. J.; Doye, J. P. K. Global optimization by basin-hopping and the lowest energy structures of Lennard-Jones clusters containing up to 110 atoms. *J. Phys. Chem. A* 1997, 101, 5111–5116.
50. Domoto, Y.; Abe, M.; Fujita, M. A highly entangled $(M_3L_2)_8$ truncated cube from the anion-controlled oligomerization of a π-coordinated M_3L_2 subunit. *J. Am. Chem. Soc.* 2021, 143, 8578–8582.